Pergamon

Journal of Structural Geology, Vol. 18, No. 4, pp. 443 to 450, 1996

0191-8141/96 $15.00 + 0.00

0191-8141(95)00064-X

Influence of mechanical stratigraphy on folding vs faulting

S. GREGG ERICKSON*

Department of Earth Sciences, Memorial University of Newfoundland, St John's, Newfoundland, Canada, A1B 3X5

(*Received* 22 *February* 1995; *accepted in revised form* 13 *May* 1995)

Abstract—The competing processes of folding and faulting during shortening of a layered sequence are investigated using elastic–plastic models, in order to determine the influence of mechanical stratigraphy on the development of fold belts vs thrust belts. The models consist of a strong middle layer and weaker décollement and cover layers. The mechanical behaviour of each layer is determined by its plastic hardening modulus h and its elastic shear modulus G. With bonded contacts, fold amplification at low shortening strain (relatively large h) is greatest for a thin cover layer and a thick décollement layer. At higher shortening strain ($h \ll G$), the middle layer may reach its peak strength before the other layers, causing it to become relatively weaker in shortening and causing fold amplification to be greatest for a thick middle layer. Free-slip contacts between the layers enhance folding and fold amplification is greatest if the slip surfaces are roughly equally distributed throughout the sequence. A relatively weak décollement layer enhances folding, consistent with the fact that fold belts usually include a salt décollement layer. Dominant wavelengths increase with increasing strength contrasts between the layers and with increasing thicknesses of the décollement and strong layers.

INTRODUCTION

Layered sequences of rock subjected to layer-parallel shortening may either fold or fault. Some regions of shortening, such as the Idaho–Wyoming–Utah thrust belt (Armstrong & Oriel 1965) and southern Appalachian thrust belt (Rich 1934, Harris & Milici 1977), have deformed primarily by faulting. Other regions, such as the central Appalachian Plateau (Gwinn 1964), Jura (Pierce 1966) and Parry Islands (Harrison & Bally 1988), have deformed primarily by folding. These differing styles of deformation may be the result of differing mechanical stratigraphy (strengths and thicknesses of layers). The stratigraphic sequences within many fold and thrust belts consist of a weak décollement layer of shale or salt, a strong layer of carbonate rocks, and a cover layer of clastic rocks (Woodward & Rutherford 1989, Goff 1990). The style of deformation is determined by both strong and weak layers within the sequence (Woodward & Rutherford 1989). Because salt may be 1–2 orders of magnitude weaker than other rock types, a salt décollement layer at the base of a fold-and-thrust belt has a large effect on the deformation and geometry of the belt (Davis & Engelder 1985). Regions dominated by folding are commonly underlain by a layer of salt (Pierce 1966, Sherwin 1972, Wiltschko & Chapple 1977, Harrison & Bally 1988) and the flow of weak material into the cores of anticlines may be necessary for the development of detachment folds (Wiltschko & Chapple 1977). The thickness of the cover layer may also determine whether folding or faulting dominates (Willis 1894). Slip surfaces within a sequence are also important, causing the sequence to behave as a multilayer rather than a single layer and thereby enhancing folding over faulting (Johnson 1980).

A three-layer model of a fold or thrust belt, which incorporates a décollement layer, strong layer and cover layer, is presented here in order to investigate the influence of mechanical stratigraphy on folding vs faulting. A similar three-layer model, with viscous material properties, was used by Goff (1990) to explain spacing of thrust-fault ramps in terms of folding instabilities. According to this interpretation, ramp spacings in thrust belts are analogous to fold wavelengths (Goff 1990). The current analysis is based on the approach of Johnson (1980), who studied the folding and faulting of single layers and multilayers of elastic–plastic materials. In this approach, material response is a competition between folding and faulting; loading conditions and material properties determine which response occurs. The current study extends the analysis to multilayers of finite thickness, instead of layers embedded within infinite media, and investigates the effects of layer strengths and thicknesses, as well as interlayer slip, on the development of fold belts vs thrust belts.

ANALYSIS

This section summarizes the analysis and explains the significance of the parameters. The derivations of the equations for displacements and stresses are given in the Appendix. In the analysis, deformation is separated into mean and perturbing parts (Johnson 1980). The mean part of the deformation represents uniform shortening,

*Present address: U.S. Peace Corps, Box 582, Banjul, The Gambia, West Africa.

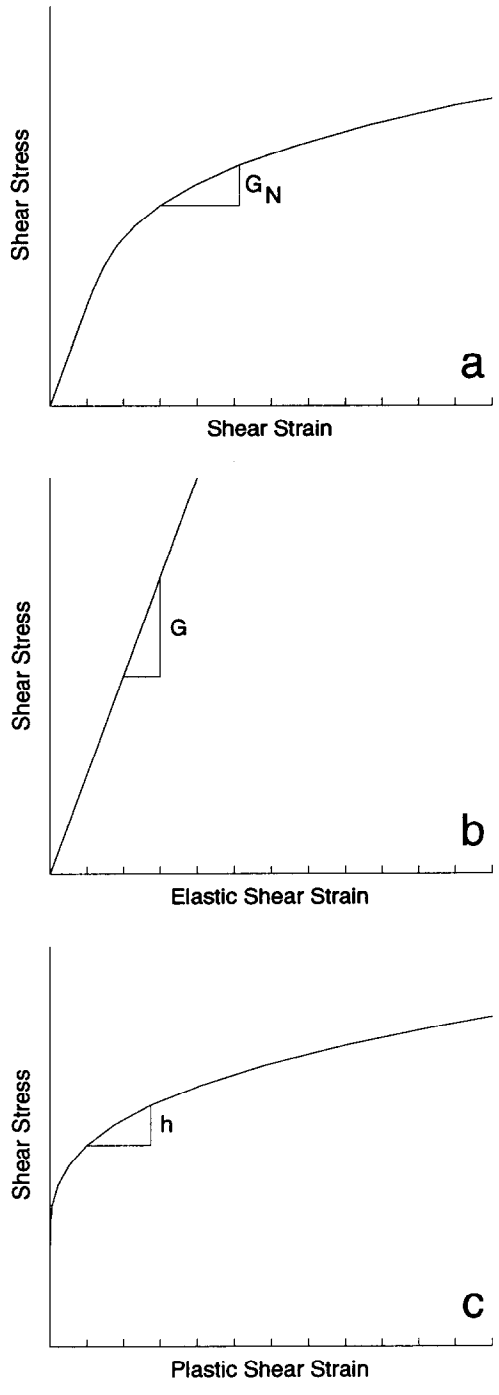

Fig. 1. Schematic stress–strain curves for an elastic–plastic material. (a) Relationship between shear stress and shear strain, with slope G_N (the tangent modulus). The shear strain can be divided into (b) an elastic part, whose relationship with shear stress is characterized by slope G (the elastic shear modulus) and (c) a plastic part, whose relationship with shear stress is characterized by slope h (the plastic hardening modulus).

whereas the perturbing part represents the growth of fold instabilities. For an elastic–plastic material, the strain can be divided into elastic and plastic components (Fig. 1) and the total, elastic and plastic strains are characterized by the moduli G_N, G and h, respectively. G_N is the tangent modulus (slope of the shear stress–shear strain curve; Fig. 1a), G is the elastic shear modulus (Fig. 1b), and h is the plastic hardening modulus (slope of the shear stress–plastic shear strain curve; Fig. 1c). G_N is related to G and h by

$$G_N = Gh/(G + h). \quad (1)$$

In the models, G is assumed to be constant, whereas G_N and h are decreasing functions of strain. In addition to G and h, the other parameter in the analysis is P, the differential axial stress, which is defined in equation (A2b) and computed by numerical integration of

$$dP/d\bar{\varepsilon}_{xx} = 4G_N, \quad (2)$$

based on the stress–strain curves.

According to this analysis, folding is possible if a perturbation amplifies significantly. If a perturbation does not amplify at a shortening strain less than that for for which $h \rightarrow 0$ (peak strength), then faulting is interpreted to occur. Plane strain is assumed, the material is incompressible and there are no density differences between the layers. Both elastic and plastic strains are assumed to be infinitesimal and the analysis is valid only for incipient buckling (Johnson 1980). Thus, this analysis cannot be used to determine final stresses and strains within the layers, but can be used to determine whether folding or faulting is most likely.

Elastic–plastic materials behave anisotropically, with G_N as the normal modulus and G as the shear modulus (equation A1). If $G \ll h$ then $G_N \rightarrow G$ (equation 1), so that the material behaves as an isotropic elastic material with modulus G. On the other hand, if $G \gg h$ the material behaves as an anisotropic material with modulus G in shear parallel to x and z and modulus G_N in shortening or extension parallel to x and z (Fletcher 1974, Johnson 1980). Because G_N decreases with increasing strain, an elastic–plastic material becomes more anisotropic with increasing strain. The forms of the governing equations for elastic–plastic materials are similar to those for viscous materials (e.g. Fletcher 1974, Goff 1990); linear viscous materials are analogous to elastic materials ($h \gg G$) and power-law viscous materials are analogous to elastic–plastic materials ($h \ll G$). Elastic–plastic and power-law viscous materials display more complex behavior than linear elastic or linear viscous materials, because the constitutive relationships are nonlinear (Smith 1979).

The three-layer model (Fig. 2) consists of a décollement layer (layer 1), a strong layer (layer 2) and a cover layer (layer 3). Each interface between the layers is given a small initial sinusoidal perturbation. These perturbations amplify into folds fastest for some dominant wavelength that depends on material properties, layer thicknesses and boundary conditions. Boundary conditions are applied at the interface between layers and at the top and bottom of the model. Layer interfaces are assumed to be either bonded, in which case the displacements and stresses must match across the interface, or free-slip, in which case the shear stress is zero along the interface. The top surface of the models is stress-free. The bottom surface is a free-slip surface with no vertical displacement, which simulates a detachment surface overlying a rigid basement. The amplification ratio used

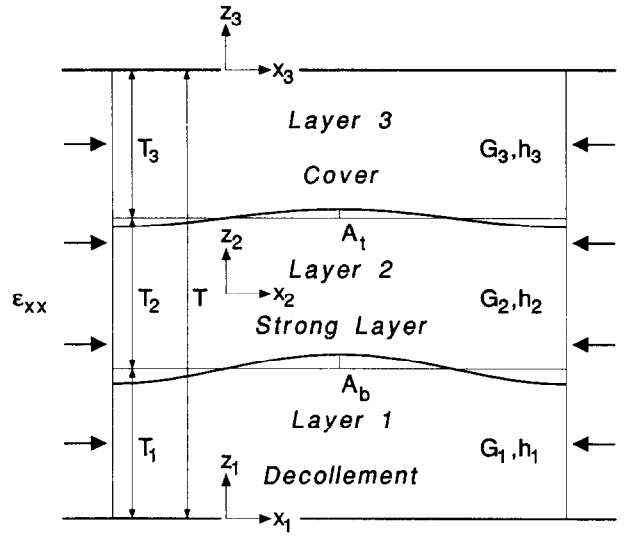

Fig. 2. Geometry of the models, showing thicknesses and material properties of layers 1 (décollement), 2 (strong layer) and 3 (cover). The top boundary is a stress-free surface and the bottom boundary has zero vertical displacement and zero shear stress.

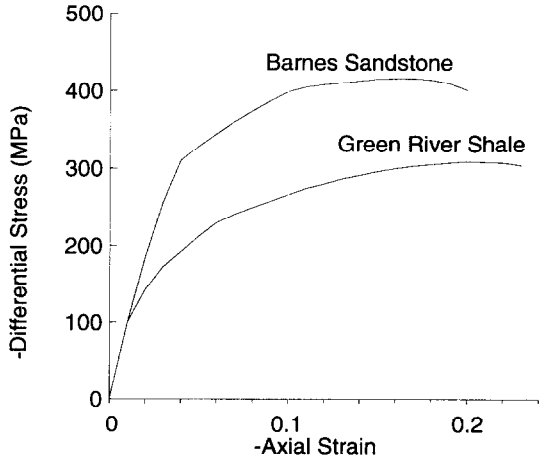

Fig. 3. Experimental stress–strain curves of Barnes Sandstone and Green River Shale at 200 MPa confining pressure (from Handin & Hager 1957). The slope of the stress–strain curves is equal to $3G_N$ for these loading conditions.

here is the average of the amplitude ratios of the two layer interfaces, $(A_t/A_{to} + A_b/A_{bo})/2$, where an o subscript represents the initial amplitude and A_t and A_b are defined in Fig. 2.

For the present study, the material properties h and G are the same as those used by Johnson (1980), based on experimental deformation (Handin & Hager 1957) of Barnes Sandstone (for layer 2) and Green River Shale (for layers 1 and 3; Fig. 3). At high shortening strain, $G \gg h$ for these materials. Barnes Sandstone reaches peak strength at a lower shortening strain ($\bar{\varepsilon}_{xx} = 0.16$) than Green River Shale, so that the 'stronger' Barnes Sandstone is relatively weaker in shortening at high strains ($G_{N1}/G_{N2} = 3.47$ at $\bar{\varepsilon}_{xx} = 0.16$; Table 1). At lower shortening strains, Barnes Sandstone is relatively stronger in shortening ($G_{N1}/G_{N2} = 0.50$ at $\bar{\varepsilon}_{xx} = 0.10$) as well as in shear ($G_1/G_2 = 0.43$). Material parameters are normalized to G_2, because the relative rather than absolute values of the parameters determine the mechanical behavior.

In the models presented here, the effects of material properties and interlayer slip are investigated as functions of layer thicknesses T_1, T_2 and T_3, which are normalized to the total thickness T. For each set of models, amplification ratio and dominant wavelength are plotted on ternary diagrams of the layer thicknesses, which cover all possible combinations of relative thicknesses. Locations on the ternary diagrams are identified using the coordinates (T_1, T_2, T_3). In two sets of models, the properties of Barnes Sandstone are used for layer 2 and those of Green River Shale are used for the weaker layers 1 and 3 (Table 1). A third set of models investigates the effects of a relatively weaker décollement layer by using values of h_1/G_2 and P_1/G_2 that are lower by a factor of 10, which approximates a layer with the mechanical properties of salt. The amplification ratios for each set of models are determined for a relatively low shortening strain ($\bar{\varepsilon}_{xx} = 0.10$) and for a shortening strain near the peak strength of Barnes Sandstone ($\bar{\varepsilon}_{xx} = 0.16$).

RESULTS

Model set I has bonded contacts and the material properties of Barnes Sandstone for layer 2 and those of Green River Shale for layers 1 and 3 (Table 1). At shortening strain $\bar{\varepsilon}_{xx} = 0.10$, fold amplification is highest for a thin cover layer and approximately equal thicknesses of strong and décollement layers ($0.45T$, $0.50T$, $0.05T$). However, fold amplification is low for all combinations of relative thicknesses, reaching a maximum of 0.5 (Fig. 4a). A thin or nonexistent cover layer enhances folding because the presence of the stress-free upper surface is equivalent to having an infinitely weak medium above that surface, making the cover layer unnecessary as a weak upper medium. At shortening strain $\bar{\varepsilon}_{xx} = 0.16$, the fold amplification is large (>100) for a thick layer 2 and thin décollement and cover layers (Fig. 4b), because layer 2 at this shortening strain has become relatively weak in shortening. The dominant wavelength at $\bar{\varepsilon}_{xx} = 0.16$ increases with increasing thicknesses of both the décollement and strong layers (Fig. 4c) to a maximum of $2.9T$ at ($0.90T$, $0.05T$, $0.05T$). This maximum dominant wavelength increases for increasing strength contrasts between the layers, to $3.4T$ if h_1/G_2, h_3/G_2, P_1/G_2 and P_3/G_2 are reduced by a factor of 10 and $4.5T$ if h_1/G_2, h_3/G_2, P_1/G_2 and P_3/G_2 are reduced by a factor of 100.

Model set II has free-slip contacts and the same material properties as model set I (Table 1). With free-slip contacts between the layers, fold amplification is greatest if the three layers have roughly the same thickness. For example, at shortening strain $\bar{\varepsilon}_{xx} = 0.10$, the fold amplification ratio (Fig. 5a) reaches a maximum at ($0.50T$,$0.25T$,$0.25T$). At shortening strain $\bar{\varepsilon}_{xx} = 0.16$, the fold amplification ratio is high for thick layers 1 and 2 and thin layer 3 (Fig. 5b). The range of relative layer

Table 1. Material properties and types of contacts used in the models. G_1/G_2 and G_3/G_2 are 0.433 for all models. The material properties in the first two model sets are based on the experimental stress–strain relations in Fig. 3. Layers 1 and 3 are based on Green River Shale and layer 2 is based on Barnes Sandstone. The third model set assumes that layer 1 is a factor of ten weaker than Green River Shale

	h_1/G_2	h_2/G_2	h_3/G_2	P_1/G_2	P_2/G_2	P_3/G_2	G_{N1}/G_{N2}	G_{N3}/G_{N2}
Model set I: bonded contacts								
$\bar{\varepsilon}_{xx} = 0.10$	0.006	0.012	0.006	−0.009	−0.016	−0.009	0.502	0.502
$\bar{\varepsilon}_{xx} = 0.16$	0.004	0.001	0.004	−0.012	−0.018	−0.012	3.472	3.472
Model set II: free-slip contacts								
$\bar{\varepsilon}_{xx} = 0.10$	0.006	0.012	0.006	−0.009	−0.016	−0.009	0.502	0.502
$\bar{\varepsilon}_{xx} = 0.16$	0.004	0.001	0.004	−0.012	−0.018	−0.012	3.472	3.472
Model set III: bonded contacts, weak layer 1								
$\bar{\varepsilon}_{xx} = 0.10$	0.0006	0.012	0.006	−0.0009	−0.016	−0.009	0.050	0.502
$\bar{\varepsilon}_{xx} = 0.16$	0.0004	0.001	0.004	−0.0012	−0.018	−0.012	0.347	3.472

thicknesses having high fold amplification is larger than that for model set I at both $\bar{\varepsilon}_{xx} = 0.10$ and $\bar{\varepsilon}_{xx} = 0.16$, indicating that free-slip contacts between the layers enhance folding. Faulting is likely only with a thick ($>0.7T$) layer 3. In contrast to the models with bonded contacts, dominant wavelength at $\bar{\varepsilon}_{xx} = 0.16$ with free-slip contacts (Fig. 5c) is not a continuously increasing function of T_1 and T_2; there is a region of dominant wavelengths $< 2T$ for thicknesses of the three layers approximately equal. Thus, the presence of evenly spaced slip surfaces throughout the sequence reduces the dominant wavelength. The dominant wavelength reaches a maximum of $2.8T$ for large T_2. Similarly to the models with bonded contacts, the maximum dominant wavelength with free-slip contacts increases with increasing strength contrast, reaching $3.2T$, if h_1/G_2, h_3/G_2, P_1/G_2 and P_3/G_2 are reduced by a factor of 10 and $6.7T$ if h_1/G_2, h_3/G_2, P_1/G_2 and P_3/G_2 are reduced by a factor of 100.

Model set III has bonded contacts and the same material properties as model sets I and II, except that layer 1 is weaker (h_1/G_2 and P_1/G_2 reduced by a factor of 10). At shortening strain $\bar{\varepsilon}_{xx} = 0.10$, the fold amplification is high (>100) for large T_1 ($T_1 > 0.3$–0.4; Fig. 6a). Therefore, with a weak décollement layer, folding is favored by a thick décollement and develops with small amounts of shortening if the décollement layer is thick. At shortening strain $\bar{\varepsilon}_{xx} = 0.16$, the amplification ratio is high for thick layers 1 and 2. The field of high fold amplification ratio on the ternary diagram is larger (Fig. 6b) than that for model set I, indicating that a weak décollement layer enhances folding. The field of high amplification includes $T_3 < 0.8T$ and $T_1 > 0.05T$, which covers most combinations of relative layer thicknesses. The weaker décollement layer increases the dominant wavelength at $\bar{\varepsilon}_{xx} = 0.16$ for all combinations of layer thicknesses (Fig. 6c). The dominant wavelength reaches a maximum of $3.9T$ for large T_1 ($0.80T$,$0.15T$,$0.05T$).

DISCUSSION

For a strong layer embedded in infinite media, fold amplification is low unless there is interlayer slip (Johnson 1980). In the current models the top surface is stress-free and the bottom surface is a shear stress-free surface above a rigid basement, so that the models consist of a strong layer (layer 2) in finite media (layers 1 and 3). The shear stress-free surface below layer 1 acts as a slip surface, and the stress-free surface above layer 3 is equivalent to having an infinitely weak medium above it. Therefore, these surfaces that bound the finite media enhance fold amplification relative to infinite media. Even with low strength contrasts between the layers and with bonded layer interfaces, fold amplification is large for many combinations of relative layer thicknesses. If there are higher strength contrasts or free-slip contacts between the layers, folding is enhanced further.

The relative layer thicknesses in fold belts, such as the Jura, central Appalachian Plateau and Parry Islands, and thrust belts, such as Idaho–Wyoming–Utah and southern Appalachians, are similar in some ways (Fig. 7). In all of these deformed belts, the décollement layer is 5–10% of the total thickness. Because the middle and cover layers of the Jura and central Appalachian Plateau are difficult to differentiate, the sequences in these belts may act approximately as two-layer rather than three-layer sequences, and are plotted accordingly in Fig. 7. Because the models indicate that a thin cover layer enhances folding, a two-layer sequence may shorten as a fold belt, whereas a three-layer sequence with a thick cover may shorten as a thrust belt. However, the relative layer thicknesses of other folded and faulted terranes do not differ significantly; for example, the Parry Islands fold belt has similar relative layer thicknesses to those in the Tennessee and Idaho–Wyoming–Utah thrust belts. Thus, the determination of whether folding or faulting occurs may be based more on layer strengths than layer thicknesses. Fold amplification increases markedly with increasing strength contrast (compare Figs. 4 and 6). Carbonate rock instead of clastic rock as the strong layer may increase this strength contrast, if fracture is the dominant deformation mechanism and pressure solution, dislocation creep and twinning are negligible. Salt instead of shale as the décollement layer also should increase the strength contrast and cause folding instead of faulting. The main difference between fold belts, such as the Jura, central Appalachian Plateau and Parry Islands, and thrust belts, such as the southern Appalachians and Idaho–Wyoming–Utah, is that the décolle-

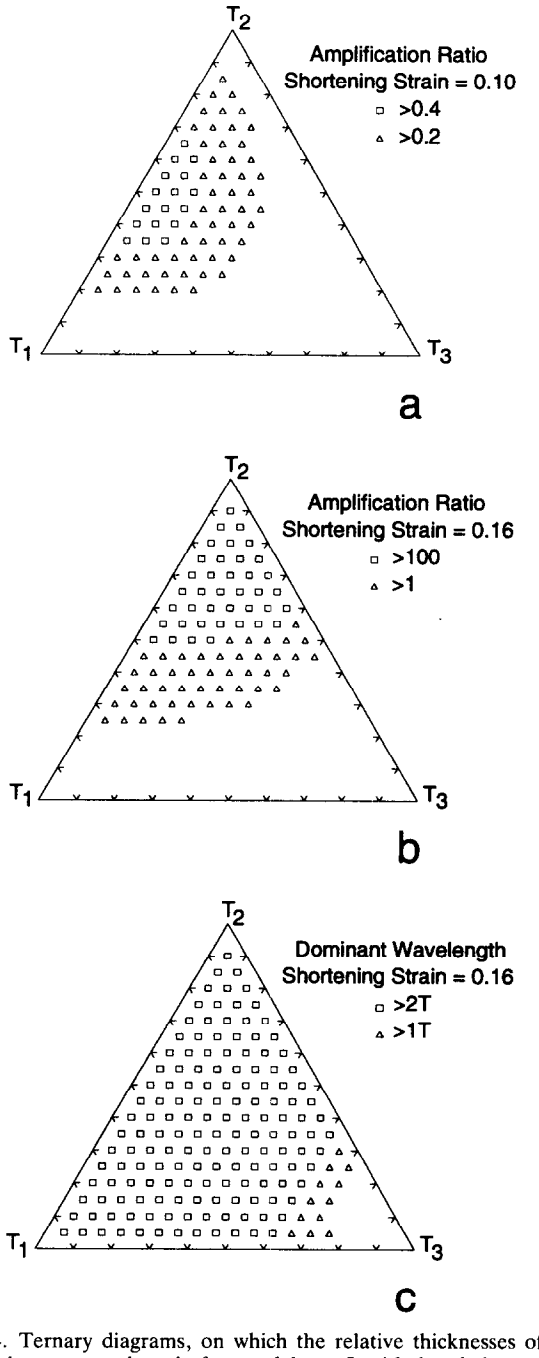

Fig. 4. Ternary diagrams, on which the relative thicknesses of the three layers are plotted, for model set I with bonded contacts. Contours of (a) amplification ratio $(A_t/A_{to} + A_b A_{bo})/2$ at shortening strain $\bar{\varepsilon}_{xx} = 0.10$, (b) amplification ratio at $\bar{\varepsilon}_{xx} = 0.16$ and (c) dominant wavelength (at $\bar{\varepsilon}_{xx} = 0.16$) relative to total thickness T, where $T = T_1 + T_2 + T_3$.

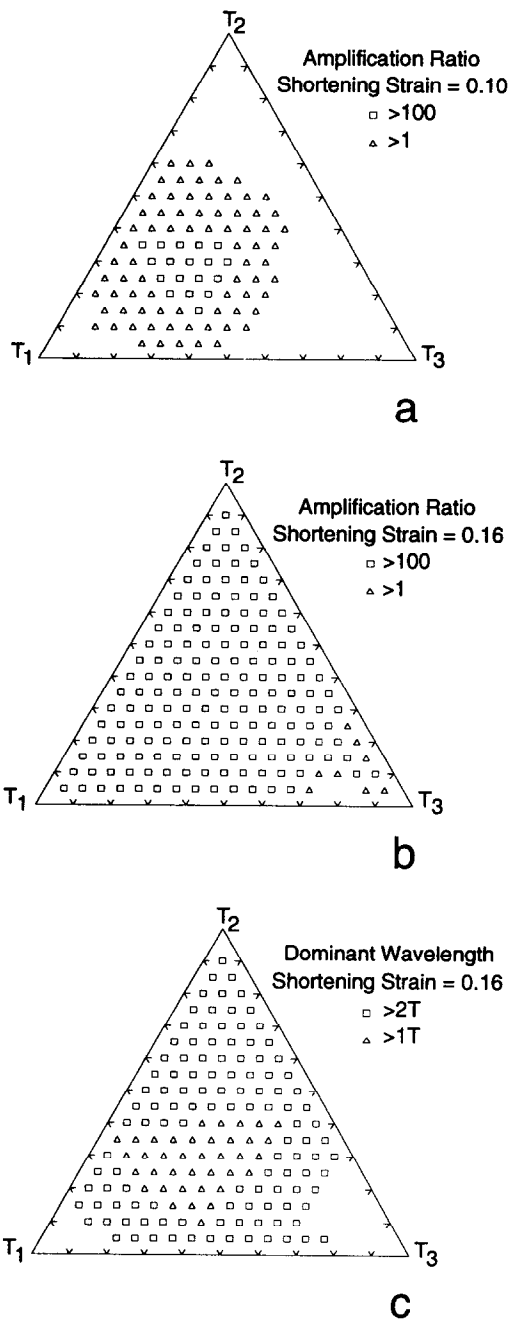

Fig. 5. Ternary diagrams of model set II with free-slip contacts. Contours of (a) amplification ratio at $\bar{\varepsilon}_{xx} = 0.10$, (b) amplification ratio at $\bar{\varepsilon}_{xx} = 0.16$ and (c) dominant wavelength at $\bar{\varepsilon}_{xx} = 0.16$.

ment layers in the fold belts contain salt. The presence of a salt décollement layer may be a determining factor in the development of a fold belt.

With the material properties of Barnes Sandstone and Green River Shale, the elastic–plastic models indicate dominant wavelengths of $<3T$. Higher strength contrasts between the layers result in larger dominant wavelengths, up to $6.7T$ with free-slip contacts if the strength contrast is 100. The calculated dominant wavelengths of the models agree reasonably well with wavelengths of fold belts. Wavelengths range from 1.4–3.3T in the Parry Islands fold belts (Harrison & Bally 1988), 1.2–2.0T in the Jura (Pierce 1966), and 2.1–7.8T in the central Appalachian Plateau (Wiltschko & Chapple 1977), where T is the total stratigraphic thickness. In the central Appalachian Plateau, large wavelengths correspond to a thick or weak (i.e. large percentage of salt) décollement layer (Wiltschko & Chapple 1977). This relationship is consistent with the models (Fig. 6c), in which dominant wavelength increases with a thicker or weaker décollement layer 1. If the spacing of thrust-fault ramps is determined by a folding instability, then the dominant wavelength may represent this ramp spacing in thrust belts (Goff 1990). Ramp spacing ranges from

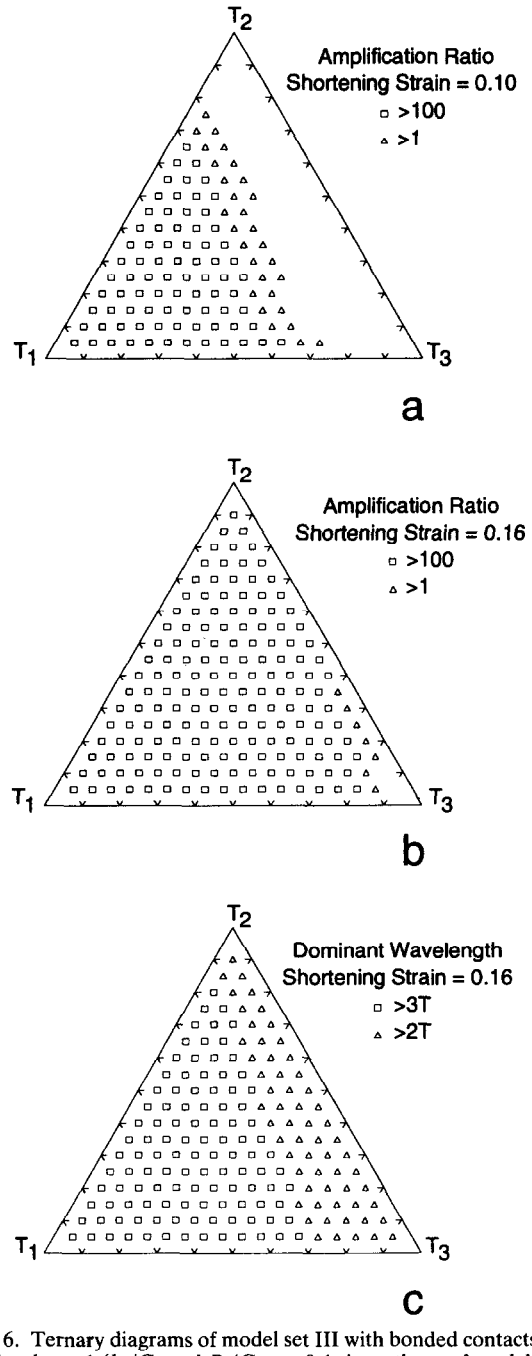

Fig. 6. Ternary diagrams of model set III with bonded contacts and a weaker layer 1 (h_1/G_2 and P_1/G_2 are 0.1 times those of model set I). Contours of (a) amplification ratio at $\bar{\varepsilon}_{xx} = 0.10$, (b) amplification ratio at $\bar{\varepsilon}_{xx} = 0.16$ and (c) dominant wavelength at $\bar{\varepsilon}_{xx} = 0.16$.

3.4–8.2T in the Idaho–Wyoming–Utah thrust belt (Goff 1990) and 5.7–13.4T in Tennessee (Woodward & Gray 1985). According to the models, these large wavelengths require a large strength contrast (>100) between the strong layer and décollement and cover layers. A similar conclusion was reached by Goff (1990); a high viscosity contrast is required to explain the ramp spacing of the Idaho–Wyoming–Utah thrust belt. Therefore, high strength contrasts are apparently necessary for the long wavelengths relative to stratigraphic thickness in thrust belts, although, based on amplification ratios, high strength contrasts should favor folding over faulting.

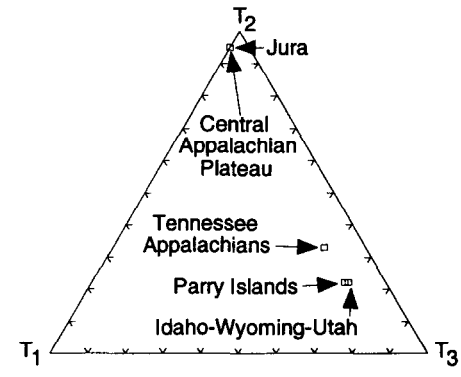

Fig. 7. Ternary diagram of the relative layer thicknesses of some fold and thrust belts. Because strong and cover layers for the Jura and central Appalachian Plateau are difficult to define, these belts are plotted at $T_3 = 0$.

CONCLUSIONS

The influence of mechanical stratigraphy on folding and faulting of a three-layer sequence has been investigated. The models indicate that high strength contrasts, a weak décollement layer, a thin cover layer and free-slip contacts between the layers enhance folding over faulting. Belts of shortening that are dominated by folding commonly have a salt décollement layer, which results in a high strength contrast with the overlying rock, indicating that the presence of a salt décollement is a key factor in producing a fold belt. At low strain and with bonded contacts, fold amplification is greatest if the décollement layer is thick. At high strain ($h \ll G$), fold amplification is greatest for a relatively thick strong layer, because the strong layer reaches peak strength before the other layers and thus becomes weaker in shortening. With free-slip contacts, folding is most likely if slip surfaces are roughly equally distributed throughout the sequence. Dominant wavelengths generally increase with increasing thicknesses of the strong and décollement layers and with increasing strength contrasts between the strong layer and the décollement and cover layers. The calculated dominant wavelengths are consistent with wavelengths in fold belts and ramp spacing in thrust belts, although they require a high strength contrast for thrust belts.

Acknowledgements—This paper benefited from the comments of Tom Tharp, Peter Hudleston and an anonymous reviewer.

REFERENCES

Armstrong, F. C. & Oriel, S. S. 1965. Tectonic development of Idaho–Wyoming thrust belt. *Bull. Am. Ass. Petrol. Geol.* **49**, 1847–1866.

Davis, D. & Engelder, T. 1985. The role of salt in fold-and-thrust belts. *Tectonophysics* **119**, 67–88.

Fletcher, R. C. 1974. Wavelength selection in the folding of a single layer with power-law rheology. *Am. J. Sci.* **274**, 1029–1043.

Goff, D. F. 1990. Mechanics of thrust-ramp spacing. Ph.D. dissertation, Texas A&M University, U.S.A.

Gwinn, V. 1964. Thin-skinned tectonics in the Plateau and northwestern Valley and Ridge provinces of the central Appalachians. *Bull. geol. Soc. Am.* **75**, 863–900.

Handin, J. & Hager, R. V. 1957. Experimental deformation of sedimentary rocks under confining pressure: tests at room temperature on dry samples. *Bull. Am. Ass. Petrol. Geol.* **41**, 1–50.
Harris, L. D. & Milici, R. C. 1977. Characteristics of thin-skinned style of deformation in the southern Appalachians, and potential hydrocarbon traps. *U.S. geol. Surv. Prof. Pap.* **1018**.
Harrison, J. C. & Bally, A. W. 1988. Cross-sections of the Parry Islands fold belt on Melville Island, Canadian Arctic Islands: implications for the timing and kinematic history of some thin-skinned décollement systems. *Bull. Can. Petrol. Geol.* **36**, 311–332.
Johnson, A. M. 1979. Derivation of linearized constitutive equations for plane-strain of an elastic–plastic (strain hardening) material. *U.S. geol. Surv. Open-File Rept.* **79–433**.
Johnson, A. M. 1980. Folding and faulting of strain-hardening sedimentary rocks. *Tectonophysics* **62**, 251–278.
Pierce, W. G. 1966. Jura tectonics as a décollement. *Bull. geol. Soc. Am.* **77**, 1265–1276.
Rich, J. L. 1934. Mechanics of low-angle overthrust faulting as illustrated by Cumberland thrust block, Virginia, Kentucky, and Tennessee. *Bull. Am. Ass. Petrol. Geol.* **18**, 1584–1596.
Sherwin, J. 1972. Décollement folding. Ph.D. dissertation, Brown University, Providence, Rhode Island, U.S.A.
Smith, R. B. 1979. The folding of a strongly non-Newtonian layer. *Am. J. Sci.* **279**, 272–287.
Willis, B. 1894. The mechanics of Appalachian structure. *13th Ann. Rept U.S. geol. Surv. 1891–1892*, pp. 213–281.
Wiltschko, D. V. & Chapple, W. M. 1977. Flow of weak rocks in Appalachian Plateau folds. *Bull. Am. Ass. Petrol. Geol.* **61**, 653–670.
Woodward, N. B. & Gray, D. R. 1985. Southwest Virginia, Tennessee, and northern Georgia sections. In: Valley and Ridge thrust belt: balanced structural sections, Pennsylvania to Alabama (edited by Woodward, N. B.). *Univ. Tennessee Dept. geol. Sci. Stud. Geol.* **12**, 40–53.
Woodward, N. B. & Rutherford, E. 1989. Structural lithic units in external orogenic zones. *Tectonophysics* **158**, 247–267.

APPENDIX

The derivation closely follows that of Johnson (1980). The stress–strain relationships, for the perturbing part of the deformation of a material subjected to mean stresses $\bar{\sigma}_{xx}$ and $\bar{\sigma}_{zz}$ are:

$$\tilde{\sigma}_{xx} = G_N(\partial u/\partial x) + \tilde{p}, \tag{A1a}$$

$$\tilde{\sigma}_{zz} = G_N(\partial w/\partial z) + \tilde{p}, \tag{A1b}$$

$$\tilde{\sigma}_{xz} = G(\partial w/\partial x + \partial u/\partial z) + (P/2)(\partial w/\partial x - \partial u/\partial z), \tag{A1c}$$

where u and w are the displacements in the x and z directions, respectively. G is the elastic shear modulus, h is the plastic hardening modulus, G_N is the tangent modulus defined in equation 1, and

$$\tilde{p} = (\tilde{\sigma}_{xx} + \tilde{\sigma}_{zz})/2 \tag{A2a}$$

$$P = \tilde{\sigma}_{xx} - \tilde{\sigma}_{zz}. \tag{A2b}$$

Now, define a stream function ψ such that

$$u = \partial\psi/\partial z, \tag{A3a}$$

$$w = -\partial\psi\partial x. \tag{A3b}$$

Substituting equations (A1) into the equilibrium equations and using equation (A3),

$$\partial^4\psi/\partial z^4 + 2Q(\partial^4\psi/\partial x^2\partial z^2) + R(\partial^4\psi/\partial x^4) = 0, \tag{A4}$$

where

$$Q = (4G_N - 2G)/(2G - P), \tag{A5a}$$

$$R = (2G + P)/(2G - P). \tag{A5b}$$

The sinusoidal solution to (A4) is

$$\psi = (1/l)\{a' \exp[(\alpha + \beta')lz] + b' \exp[-(\alpha + \beta')lz] + c' \exp[(\alpha - \beta')lz] + d' \exp[-(\alpha - \beta')lz]\} \cos(lx), \tag{A6}$$

where

$$\alpha = [(Q + R^{1/2})/2]^{1/2}, \tag{A7a}$$

$$\beta' = [(Q - R^{1/2})/2]^{1/2}, \tag{A7b}$$

$$l = 2\pi/L, \tag{A7c}$$

and L is the wavelength. If α and β' are imaginary, equation (A4) is hyperbolic, so that discontinuities are possible and faulting is predicted (Johnson 1980). If α is real and β' is imaginary, folding is possible if a perturbation amplifies significantly at some wavelength. Thus, according to this analysis, whether α is real or imaginary determines whether the material folds or faults. For $-P \ll G$, α is real if h is positive and imaginary if h is negative. Therefore, if the fold amplitude for some wavelength does not become large at a shortening strain less than that for which $h \to 0$, faulting is interpreted to occur rather than folding. For α real and β' imaginary,

$$w = -\partial\psi/\partial x = \{[a \sin(\beta lz) + b \cos(\beta lz)] \exp(\alpha lz) + [c \sin(\beta lz) + d \cos(\beta lz)] \times \exp(-\alpha lz)\} \sin(lx), \tag{A8a}$$

$$u = \partial\psi/\partial z = \{[(a\beta + b\alpha) \cos(\beta lz) + (a\alpha - b\beta) \sin(\beta lz)] \exp(\alpha lz) + [(c\beta - d\alpha) \cos(\beta lz) - (c\alpha + d\beta) \sin(\beta lz)] \times \exp(-\alpha lz)\} \cos(lx), \tag{A8b}$$

where

$$i\beta = \beta' = i[(R^{1/2} - Q)/2]^{1/2}. \tag{A9}$$

Equations (A8) differ from the equations of Johnson (1980) because, in the present study, the media (the décollement and cover layers) have finite thicknesses and may have differing material properties.

In order to apply boundary conditions at the layer interfaces, it is necessary to introduce a local coordinate system in which the axes are normal and parallel to the interface. The stresses at the interfaces (Johnson 1979), to first order in the slope of the interfaces, are

$$\sigma_{ns} = \tilde{\sigma}_{xz} - P(\partial w/\partial x + \partial w_o/\partial x), \tag{A10a}$$

$$\sigma_{nn} = \tilde{\sigma}_{zz} + \tilde{\sigma}_{zz}, \tag{A10b}$$

where n indicates the direction normal to the interface and s the direction parallel to the interface, w is the additional and w_o the initial vertical displacement of the interface,

$$w_o = A_o \sin(lx). \tag{A11}$$

Substituting equations (A1) and (A8) in (A10),

$$\sigma_{ns} = l(G - P/2)\{\{[(1 + Q)a - 2\alpha\beta b] \sin(\beta lz) + [2\alpha\beta a + (1 + Q)b] \cos(\beta lz)\} \exp(\alpha lz) + \{[(1 + Q)c + 2\alpha\beta d] \sin(\beta lz) + [-2\alpha\beta c + (1 + Q)d] \cos(\beta lz)\} \times \exp(-\alpha lz)\} \cos(lx) - PA_o l \cos(lx), \tag{A12a}$$

$$\sigma_{nn} = \bar{\sigma}_{zz} + l(G - P/2)\{\{[\beta(1 - R^{1/2}) \cos(\beta lz) + \alpha(1 + R^{1/2}) \sin(\beta lz)]a + [\alpha(1 + R^{1/2}) \cos(\beta lz) - \beta(1 - R^{1/2}) \sin(\beta lz)]b\} \exp(\alpha lz) + \{[\beta(1 - R^{1/2}) \cos(\beta lz) - \alpha(1 + R^{1/2}) \sin(\beta lz)]c - [\alpha(1 + R^{1/2}) \cos(\beta lz) + \beta(1 - R^{1/2}) \sin(\beta lz)]d\} \times \exp(-\alpha lz)\} \sin(lx). \tag{A12b}$$

For each jth layer, there are four constants, a_j, b_j, c_j and d_j, which are determined by the boundary conditions at the interfaces between the layers and at the top and bottom surfaces. The boundary conditions at the interface between layers j and $j + 1$ are, for a bonded interface,

$$(\sigma_{ns})_j = (\sigma_{ns})_{j+1}, \tag{A13a}$$

$$(\sigma_{nn})_j = (\sigma_{nn})_{j+1}, \tag{A13b}$$

$$u_j = u_{j+1}, \tag{A13c}$$

$$w_j = w_{j+1}. \tag{A13d}$$

For a free-slip (no shear stress) interface,

$$(\sigma_{ns})_j = 0, \tag{A14a}$$

$$(\sigma_{ns})_{j+1} = 0, \tag{A14b}$$

$$(\sigma_{nn})_j = (\sigma_{nn})_{j+1}, \tag{A14c}$$

$$w_j = w_{j+1}. \tag{A14d}$$

The boundary conditions at the lower surface are

$$w_1 = 0, \tag{A15a}$$

$$(\sigma_{ns})_1 = 0, \tag{A15b}$$

which simulates a free-slip detachment overlying a rigid basement. At the top surface,

$$(\sigma_{nn})_3 = 0, \tag{A16a}$$

$$(\sigma_{ns})_3 = 0, \tag{A16b}$$

which represents a stress-free surface. Boundary conditions (A15) require that $b_1 = -d_1$ and $a_1 = c_1$. Using these results, the system is reduced to 10 equations in 10 unknown constants a_1, b_1, a_2, b_2, c_2, d_2, a_3, b_3, c_3, d_3. Once these constants have been determined, the amplitude A can be calculated from equation (A8a), because

$$w = A \sin(lx). \tag{A17}$$